J. Fluid Mech. (2010), *vol.* 654, *pp.* 453–472.
doi:10.1017/S0022112010000613

Stroke-averaged lift forces due to vortex rings and their mutual interactions for a flapping flight model

X. X. WANG AND Z. N. WU†

Department of Engineering Mechanics, Tsinghua University, Beijing 100084, PR China

(Received 20 April 2009; revised 31 January 2010; accepted 1 February 2010; first published online 23 April 2010)

The stroke-averaged lift forces due to various vortex rings and their mutual interactions are studied using a flapping flight vortex model (Rayner, *J. Fluid Mech.*, vol. 91, 1979, p. 697; Ellington, *Phil. Trans. R. Soc. Lond.* B, vol. 305, 1984*b*, p. 115). The vortex system is decomposed into the wing plane (wing-linked) vortex ring, a loop closed by the bound vortex and (arc-shaped) trailing vortex and the wake (the vortex rings shed previously). Using the vorticity moment theory (Wu, *AIAA J.*, vol. 19, 1981, p. 432) we are able to identify the roles of vortex rings in lift production or reduction and express the lift as function of areal contraction or expansion of vortex rings. The wake vortex rings induce areal contraction of the trailing vortex, which should decrease the lift, but this decrease is exactly compensated by the inducing effect of the trailing arc on the wake. The wake reduces the lift through inducing a downwash velocity on the wing plane. The lift force is shown to drop to a minimum at the second half stroke, and then increases to an asymptotic value slightly below the lift at the first half stroke, in such a way following the experimental observation of Birch & Dickinson (*Nature*, vol. 412, 2001, p. 729). The existence of the negative peak of lift is due to the first shed vortex ring which, just at the second half stroke, lies in the close vicinity to the wing plane, leading to a peak of the wing plane downwash velocity.

1. Introduction

In addition to the conventional lift mechanism, insect flapping flight involves various additional aerodynamic mechanisms such as Weis-Fogh mechanism by the 'clap and fling' motion (Weis-Fogh 1973; Miller & Peskin 2005), wing rotation (Dickinson, Lehmann & Sane 1999; Sane & Dickinson 2002; Bergou, Xu & Wang 2007), added mass (Sane & Dickinson 2001), vortex effect (leading edge vortex, Ellington *et al.* 1996; Birch, Dickson & Dickinson 2004; Bomphrey *et al.* 2006) and wake vortices (Ramamurti & Sandberg 2007; Lehmann 2008); see Maxworthy (1981), Sane (2003), Lehmann (2004), Wang (2005) and Ansari, Zbikowski & Knowles (2006) for details and for more references. Though the importance of wakes in altering the conventional lift has been recognized (Rayner 1979; Ellington 1984*b*; Sane 2003), its specific role on aerodynamic force has not been well studied. For instance, Lehmann (2008) recently pointed out that the majority of studies on insect flight aerodynamics widely ignored the significance of wake patterns produced by previous strokes. Fortunately,

† Email address for correspondence: ziniuwu@tsinghua.edu.cn

a number of experimental and numerical studied were conducted in recent years in order to reveal the vortical structure and wake patterns in flapping flight (Bomphrey *et al.* 2006; Ramamurti & Sandberg 2007; Aono, Liang & Liu 2008; Altshuler *et al.* 2009), which may help to improve understanding about the wake influence on the aerodynamic performance.

Rayner (1979) and Ellington (1984*b*) modelled the wake of hovering insects as a chain of coaxial horizontal circular vortex rings stacked one upon another. A vortex ring is released to the wake after each half stroke and begin to move downwards in the induced velocity field. This approach deals with the averaged aerodynamic force in a stroke period.

Controversial perspectives have been proposed on the contribution of the wake to the lift force. Dickinson *et al.* (1999) proposed that wake capture may enhance lift. When the wings complete rotation and enter the wake created by the previous strokes, a transient peak in the aerodynamic force is brought by the mutual interaction between the wings and the wake. Force due to wake capture is sensitive to the details of the wing kinematics. The diverse manners in which the wings enter the wake lead to disparate consequences on aerodynamic forces. Dickinson *et al.* (1999) found in model experiments that insects benefit from their shed vorticity which may explain the large positive transient that develops immediately after the wings reverse direction at the start of each half stroke in an advanced rotation case. The same geometry and wing kinematics are adopted by Sun & Tang (2002) in their numerical simulations. In contradiction to results by Dickinson and his colleagues, the computational results have drawn to the conclusion that the peak in the lift force is due to wing acceleration. The wake produced in previous strokes has an attenuating effect on the lift force rather than an enhancing one. Birch & Dickinson (2001) have shown by experiments that the first stroke in a fruit fly model wing produces approximately 9 % more lift than the subsequent strokes where the effective angle of attack is attenuated by more than 10^{o}. Vortices play a negative role in this situation. Lehmann (2008) has reviewed the wing wake interference and pointed out that the flow induced by the preceding half strokes may lower the effective angle of attack but permits the recycling of kinetic energy from the wake.

The lack of knowledge about the specific contribution of the wake on the aerodynamics of insect flight seems to be due to the consideration of as many phenomena as possible in each of the past studies. Hence, a study about the sole influence of the wake seems to be necessary. In this paper, we will disregard the various effects other than the vortex structure and use the flapping flight vortex model by Rayner (1979) and Ellington (1984*b*) to study the role of various vortex rings and their mutual interactions on the (stroke-averaged) lift. The vortex system is composed of a wing-linked vortex ring and wakes (vortex rings shed during the previous strokes). Using the vorticity moment theory by Wu (1981), we will be able to identify the roles of various vortex rings and their mutual interactions. The vorticity moment theory relates the aerodynamic forces to the moment of distributed or distinct vortices. This allows us to express the aerodynamic force as function of strength and areal contraction of vortex rings and study the relative contribution of wing-linked vortex and wakes. The vortex model used in this paper will be presented in § 2. In § 3, the vorticity moment theory will be applied to the vortex system. In § 4 the contribution by the bound vortex, trailing vortex and wakes will be identified and the time history of the lift will be studied. Concluding remarks for this paper and perspective for future study such as unsteadiness in each stroke and body influence will be stated in § 5.

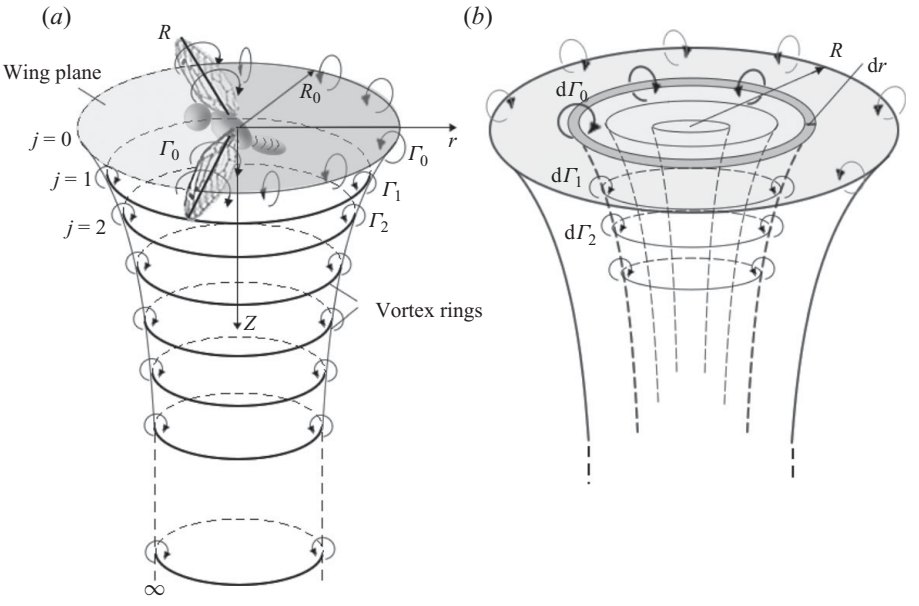

FIGURE 1. Diagrams of vortex structure for single (*a*) and multiple (*b*) chains of vortex rings.

2. Vortex rings in a flapping flight model

In this section, we first present the vortex model. Then we use the vortex method by Rayner (1979) to display some features related to the vortex ring evolution useful for aerodynamic study in the next. Finally, we will derive a formula for mutual interaction between two vortex rings.

2.1. *Vortex model*

In the flapping flight vortex model (Rayner 1979; Ellington 1984*b*) as displayed in figure 1(*a*), the vortex system is composed of a wing-linked vortex ring and wake. Normally, the circulation of the bound vortex has a distribution along the span, so that the vortex system can be more reasonably represented by the multi-chain model as displayed in figure 1(*b*) (Ellington 1984*b*). The single-chain model displayed in figure 1(*a*) and adopted in this paper can be viewed as an average of the multi-chain model, namely, a single vortex ring is used to represent the vortices in each plane. In such a way, the wing-linked vortex ring has a constant circulation along the span and trailing arc, and the radius R_0 of the wing plane vortex ring is a proportion of the wing span R. For an elliptical distribution of circulation along the span, $R_0 = (\pi/4)R$ (Gerz, Holzäpfel & Darracq 2002) while Rayner (1979) gives $R_0 = 0.7 \sim 0.8R$. The specific value of R_0/R does not have an influence on the conclusion.

The wing plane vortex ring $j = 0$ is composed of the bound vortex (straight segments along the wing spans) and trailing vortex (arc shape, see figure 2*a*) (Lauder 2001; Traub 2004). The wakes are composed of a series of vortex rings ($j = 1, 2, 3, \ldots$) previously shed from the wing plane vortex ring (see figure 2*b*) and larger j refers to earlier shedding. Each vortex ring has a circulation $\Gamma_j < 0$. Throughout this paper we will assume a constant Γ_j (in time).

The trailing arc does not appear as a complete circle. Since we are interested in the stroke-averaged lift, we will model the trailing arc as an equivalent circle with a half circulation of the bounding vortex, following Rayner (1979).

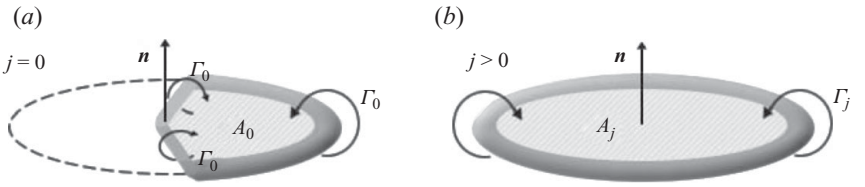

FIGURE 2. Wing plane vortex ring (a) and vortex ring in the wake (b). The former is composed of a circular arc of trailing vortex and two segments of bound vortices.

Normally, the circulation Γ_j is dependent on j. In §4, we will show that Γ_j is dependent of the stroke especially for the initially shed vortex rings, and that after a large number of strokes, Γ_j is almost independent of j for the later shed vortex rings.

The single vortex ring model we adopt here is supported by the early experimental work of Kokshaysky (1979) and Spedding (1986) in bird flight where the wake structure is reported to be a chain of planar nearly circular discrete small-cored vortex loops. In recent elaborate particle image velocimetry (PIV) experiment, Altshuler *et al.* (2009) obtained further clear evidence for chain of separate vortex loops that are shed during down and up strokes in the wake of a hovering hummingbird. Due to the hummingbird morphology and wing kinematics, two vortex rings are produced each stroke, one per wing. For general insects like hawkmoth, Bomphrey *et al.* (2006) found that a single loop is produced by both wings during a stroke in forward flight. Ramamurti & Sandberg (2007) confirmed the ring-like structure in the wake and further proposed more detailed vortical structures through numerical simulation. It is not our intention to go into the intricate details of the vortical structure in the current paper, and therefore in our vortex model, we only encompass the essential features of hovering flapping flight according to these experimental and computational results. The complicated wake patterns, including double-loop configuration in hummingbirds and bats, the non-planar elliptical shape of the vortex loops and the intricate details of vorticity field are remained for future investigation.

2.2. *Evolution of the vortex rings*

When the wings finish a half stroke, the attached or bound vortices on both wings and of the same magnitude and opposite sense cancel each other as the wings clap. The two ends of the trailing vortex line meet each other so that an enclosed vortex ring is formed. Therefore, starting from the first stroke, a vortex ring is added to the flow field each a half stroke $T/2$, where T is the stroke period. The vortex pattern displayed in figure 1 is a view at some instant.

In the following sections the force will be related to the movement of the vortex rings, so we compute here the evolution of the vortex rings, using the method proposed by Rayner (1979).

Assume now there are J vortex rings shed in the flow field. According to Rayner (1979), the vortex ring j (of strength Γ_j and radius R_j) induces, at a point $\boldsymbol{z}$ with a distance r_j to the centreline of the ring j and h_j above the plane of the ring j, a velocity of components

$$u_{rj}(\boldsymbol{z}) = \frac{R_j h_j}{\pi\left[(r_j+R_j)^2+h_j^2\right]^{3/2}}\frac{\Gamma_j}{e_{r_j}^2}\left(\frac{2-e_{r_j}^2}{1-e_{r_j}^2}E(e_{r_j})-2K(e_{r_j})\right), \tag{2.1a}$$

$$u_{zj}(\boldsymbol{z}) = \frac{R_j^2\Gamma_j}{\pi\left[(r_j+R_j)^2+h_j^2\right]^{3/2}}\left[\frac{E(e_{r_j})}{1-e_{r_j}^2}-\frac{r_j}{e_{r_j}^2R_j}\left(\frac{2-e_{r_j}^2}{1-e_{r_j}^2}E(e_{r_j})-2K(e_{r_j})\right)\right], \tag{2.1b}$$

where $K(e)$ and $E(e)$ are complete elliptic integrals of first and second kind, with eccentricity e defined as $e_{r_j}^2 = (4r_j R_j)/[(r_j + R_j)^2 + h_j^2]$.

If we normalize the velocity by

$$V_m = \pi R_0 / T \tag{2.2}$$

and the lengths R_j, r_j, h_j by R_0, then (2.1a) and (2.1b) can be rewritten as

$$\bar{u}_{rj}(z) = \frac{4f\bar{R}_j\bar{h}_j}{\left[(\bar{r}_j + \bar{R}_j)^2 + \bar{h}_j^2\right]^{3/2}} \frac{\Gamma_j}{\Gamma_0} \frac{1}{\bar{e}_{r_j}^2} \left(\frac{2 - \bar{e}_{r_j}^2}{1 - \bar{e}_{r_j}^2} E(\bar{e}_{r_j}) - 2K(\bar{e}_{r_j}) \right), \tag{2.3a}$$

$$\bar{u}_{zj}(z) = \frac{4f\bar{R}_j^2}{\left[(\bar{r}_j + \bar{R}_j)^2 + \bar{h}_j^2\right]^{3/2}} \frac{\Gamma_j}{\Gamma_0} \left[\frac{E(\bar{e}_{r_j})}{1 - \bar{e}_{r_j}^2} - \frac{r_j}{\bar{e}_{r_j}^2 R_j} \left(\frac{2 - \bar{e}_{r_j}^2}{1 - \bar{e}_{r_j}^2} E(\bar{e}_{r_j}) - 2K(\bar{e}_{r_j}) \right) \right], \tag{2.3b}$$

where $\bar{e}_{r_j}^2 = (4\bar{r}_j\bar{R}_j)/[(\bar{r}_j + \bar{R}_j)^2 + \bar{h}_j^2]$ and the over bar denotes the non-dimensional value. In the above equations,

$$f = -\Gamma_0 T / \left(4\pi^2 R_0^2\right) \tag{2.4}$$

is the feathering parameter (Rayner 1979), defined as the square of ratio between the downwash velocity at the wing plane and the mean wing tip velocity. For typical insects, Rayner (1979) gives $f = 0.005$–0.015.

Summing up the induced velocity over all the vortex rings in the flow field gives the final downward velocity u_{zi} and the contraction velocity u_{ri} for the vortex ring i:

$$u_{zi} = \sum_{j=0}^{J} u_{zj}(z_i), \quad u_{ri} = \sum_{j=0}^{J} u_{rj}(z_i) \tag{2.5}$$

with the z-axis pointing downwards; positive u_{zi} refers to downwash. The centre position z_i and radius R_i of the vortex ring i is then computed as

$$\mathrm{d}z_i/\mathrm{d}t = u_{zi}, \quad \mathrm{d}R_i/\mathrm{d}t = u_{ri}. \tag{2.6}$$

Now we will analyse the trajectories of vortex rings based on a Γ_j independent of j. For Γ_j varying with j, we will show in § 4 that the results do not change much. Equation (2.6) along with (2.1a) and (2.1b) is solved using a forth-order Runge–Kutta method, with a time step carefully chosen so that further increasing the numerical accuracy does not affect the results.

Figure 3 displays the shed vortex ring trajectories at different instants when $f = 0.005$. In figures 3(a) and 3(b), the numbers (such as 1, 2 and 3) represent ring index j. Larger indices refer to earlier shed vortex rings. We observe that the vortex rings shed during the early times move in a disordered way, see from figure 3(a) the trajectory after five half strokes. For the two first shed vortex rings, the rearward ring is drawn through the centre of the forward ring, and the rings pass back and forth through one another. Such a process has been discussed by Batchelor (1967) for two vortex rings.

After a great number of strokes, the previously shed vortex rings have gradually developed steady induced velocity field beneath the wing disk, so that the motion of the newly shed vortex ring due to the induced velocity becomes steady and ordered. It can be seen from figure 3(b) that, after about seven half strokes, the newly shed vortex rings have already show signs of orderly motion. The vortex rings immediately beneath the stroke plane arrange in order and their trajectories are no longer helical. At this moment, the early vortex rings still move disorderly in the near field, however,

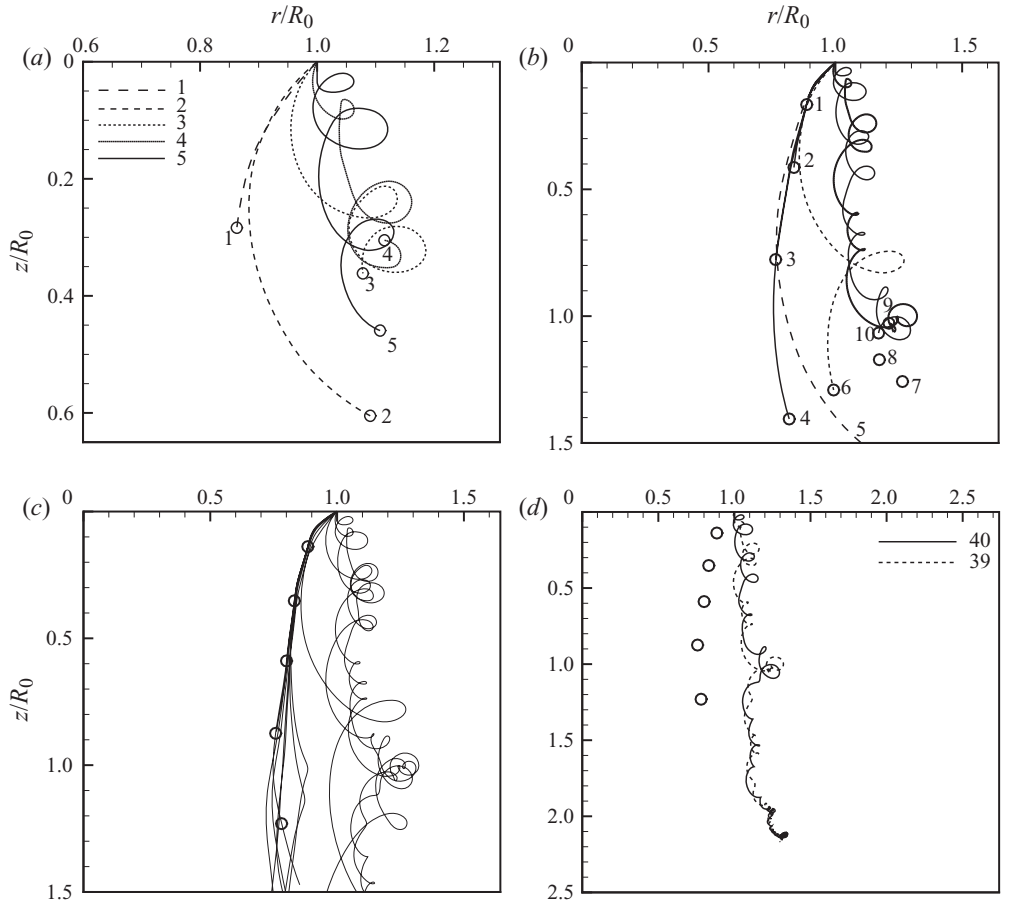

FIGURE 3. Vortex ring trajectories after they are shed when $f = 0.005$. (*a*) Five half strokes, (*b*) 10 half strokes, (*c*) 40 half strokes, (*d*) 40 half strokes with only the trajectories of the two earliest shed vortex rings shown. ○ indicates vortex ring positions and the numbers indicate their indices j.

their instability seems to have little impact on the stable distribution of the vortex rings just beneath the stroke plane.

Figure 3(*c*) is the vortex ring trajectory after 40 half strokes. This time duration is long enough for a stable ring distribution to form beneath the stroke plane, so that this vortex ring distribution can be taken as the stable state case. Vortex rings marked by ○ constitute the steady wake shape beneath the wings. The areal contraction ratio no longer changes with time. This steady portion of vortex wake prolongs as the flapping motion proceeds. A comparison between figures 3(*b*) and 3(*c*) shows that after 10 half strokes, the paths of the newly shed vortex rings has already resemble that in a stable wake, indicating that it does not take long for the vortex rings to form a relatively definite path of downward movement.

Figure 3(*d*) focuses on the unstable vortex rings shed in the early stage of flapping. Take the first and second shed vortex rings ($j = 40$ and 39) as an example. As the flapping motion proceeds, they move further downwards. After 40 half strokes, they have already moved far apart from the stroke plane. Although position and radius of these vortex rings still vary substantially with time, their influence on the flow

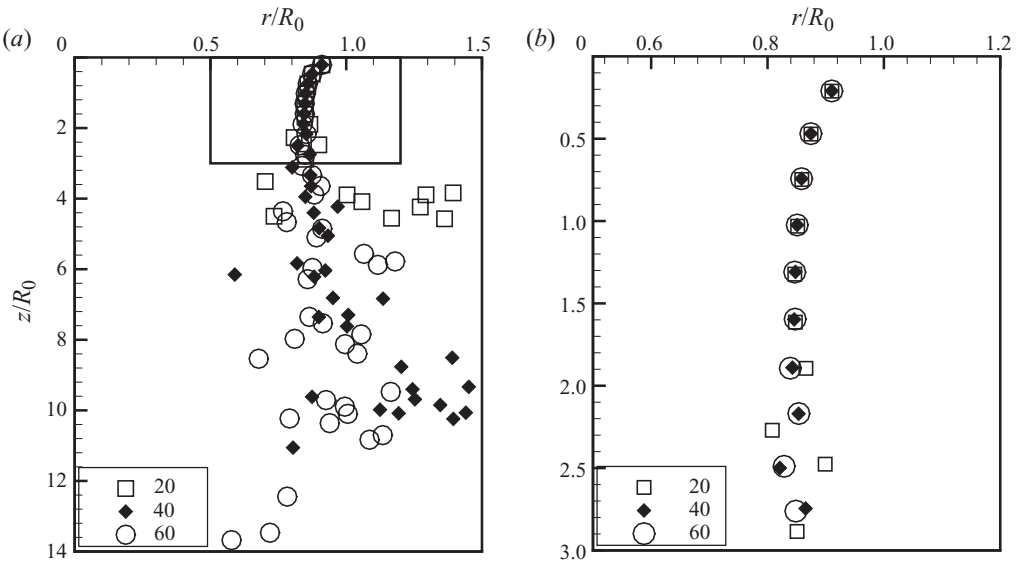

FIGURE 4. Vortex ring position after 20, 40, 60 half strokes. (*a*) Whole view, (*b*) self-consistency part.

near the stroke plane is gradually weakening. As these two vortex rings move further downstream, their trajectory get closer to each other, leading to amalgamation as observed by Maxworthy (1972) for two vortex ring system. The newly shed vortex rings travel and deform to become the next in the chain, and an additional ring is added to the wake from the wing disk. This leads to self-consistency as defined by (Rayner 1979). If we look at the time history of this self-consistent system, a vortex ring deforms into itself over a single wing cycle. Any member of the family of rings travels and deforms to become the next in the chain, and a further ring is added on the wing disk. The assumption of self-consistent system is valid only after a large number of (half) strokes.

Figure 4 displays the results for $f = 0.015$, after the wings have experienced 20, 40, 60 half stokes. In the immediate vicinity of the stroke plane, distribution of rings are basically the same for the three cases of stoke number, indicating that self-consistency has already established in 20 half strokes. With respect to the case $f = 0.005$, steady state or self-consistency in the close vicinity of the wing is reached more fast for $f = 0.015$.

2.3. *Mutual induction between vortex rings*

In the next sections, we will characterize the force using the combination $R_j \Gamma_j u_{kj}$. Here u_{kj} is the radial contraction velocity of the jth vortex ring induced by the kth vortex ring. Assume that the two vortex rings j and k are separated by a distance h_{kj}, then u_{kj} is given by

$$u_{kj} = \frac{4 f R_k h_{kj}}{\left[(R_k + R_j)^2 + h_{kj}^2\right]^{3/2}} \frac{\Gamma_k}{\Gamma_0} \frac{1}{e_{kj}^2} \left(\frac{2 - e_{kj}^2}{1 - e_{kj}^2} E(e_{kj}) - 2K(e_{kj}) \right) \tag{2.7}$$

according to (2.1*a*). Here $e_{kj}^2 = (4R_k R_j)/[(R_k + R_j)^2 + h_{kj}^2]$.

For the vortex ring j, the total radial velocity at R_j induced by all the other vortex rings is given by

$$u_{R_j} = u_{0j} + \sum_{k=1,k\neq j}^{\infty} u_{kj}. \tag{2.8}$$

Using (2.7), one can easily prove that the mutual induced velocity of the two vortex rings satisfies the relation

$$R_k \Gamma_k u_{jk} + R_j \Gamma_j u_{kj} = 0 \tag{2.9}$$

so that the following equality holds:

$$\sum_{j=1}^{\infty} \sum_{k=1,k\neq j}^{\infty} R_j \Gamma_j u_{kj} = 0. \tag{2.10}$$

If the trailing vortex arc is averaged over a stroke, it can be regarded as a vortex ring of radius R_0 but with a half-circulation. For the half-circulation ring it holds

$$R_0 \Gamma_0 u_{j0} + 2R_j \Gamma_j u_{0j} = 0. \tag{2.11}$$

Since the bounding vortex segments will pass any point of the wing plane at two instants of equal duration but with opposite signs, its inducing effect on the wake, when stroke-averaged, is negligible and not considered here. If one would study the unsteadiness inside each stroke, this inducing effect should be considered.

3. Aerodynamic forces linked to the vortex rings

Now we apply the vorticity moment theory proposed by Wu (1981) to build expressions of aerodynamic forces related to the system of vortex rings.

3.1. *Vorticity moment theory*

The vorticity moment theory developed by Wu (1981) is applicable to a general viscous and unsteady flow around accelerating and deformable bodies. Consider an infinitely large domain which is jointly occupied by the fluid and the solid body. The coordinate is chosen so that the fluid in the infinity is quiescent. According to Wu (1981), the instantaneous aerodynamic force F exerted on the immersed body is related to the vorticity moment by

$$\boldsymbol{F} = -\frac{\rho}{2}\frac{\mathrm{d}}{\mathrm{d}t} \iiint_{R_f} \boldsymbol{r} \times \boldsymbol{\omega} \mathrm{d}R + \rho \frac{\mathrm{d}}{\mathrm{d}t} \iiint_{R_s} (\boldsymbol{v} + \boldsymbol{\Omega} \times \boldsymbol{r}) \mathrm{d}R \tag{3.1}$$

where ρ is the fluid density, $\boldsymbol{v}$ is the velocity vector of the solid, $\boldsymbol{\omega}$ is the vorticity, $\boldsymbol{\Omega}$ is the angular velocity of the solid body, $\boldsymbol{r}$ is the position vector in the three-dimensional space, R_f is the region occupied by the fluid and R_s is the region occupied by the solid body.

The first term in (3.1), namely

$$\boldsymbol{F}_{\Omega} = -\frac{\rho}{2}\frac{\mathrm{d}}{\mathrm{d}t} \iiint_{R_f} \boldsymbol{r} \times \boldsymbol{\omega} \mathrm{d}R \tag{3.2}$$

is the aerodynamic force exerted on the solid body due to time variation of vorticity moment. The second term describes the force due to the acceleration or deformation of the solid body. Only the first term is directly related to the vortex rings considered in this paper and will be retained in the present study since we disregard the various additional effects other than the vortex structure.

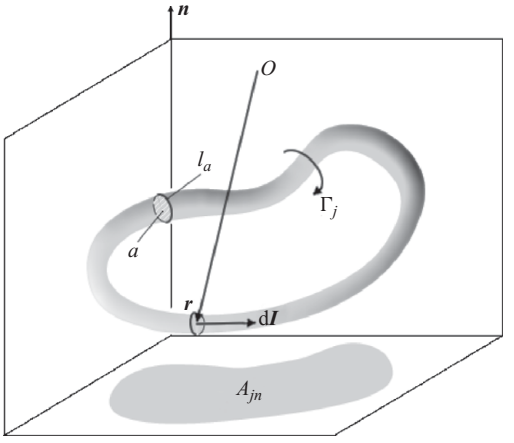

FIGURE 5. Illustration of a vortex ring in the three-dimensional space.

Applying the expression (3.2) to the vortex ring system of figure 1 and considering that $\boldsymbol{F}_\Omega$ is linear with respect to $\boldsymbol{\omega}$, we obtain

$$\boldsymbol{F}_\Omega = \sum_j \boldsymbol{F}_{\Omega_j}, \tag{3.3}$$

where

$$\boldsymbol{F}_{\Omega_j} = -\frac{\rho}{2}\frac{\mathrm{d}}{\mathrm{d}t}\iiint_{R_{f_j}} \boldsymbol{r}\times\boldsymbol{\omega}\mathrm{d}R \tag{3.4}$$

is the term related to the jth vortex ring in the flow field.

3.2. *Aerodynamic force related to an arbitrary-shaped vortex ring*

Now we derive the explicit form of $\boldsymbol{F}_{\Omega_j}$ due to each vortex ring. Though each vortex ring lies in a plane for the problem considered in this paper, we will derive the expression for an arbitrary-shaped vortex ring. Consider an enclosed vortex tube of arbitrary shape in three-dimensional flow field, whose vorticity concentrates in an infinitely small core, as illustrated in figure 5. By definition we have

$$\iint_a \boldsymbol{\omega}\cdot\boldsymbol{n}_a\mathrm{d}A = \oint_{l_a} \boldsymbol{v}\cdot\mathrm{d}\boldsymbol{s} = \Gamma_j, \tag{3.5}$$

where $\boldsymbol{v}$ is the velocity vector of the fluid, a is the cross-section of the vortex tube, $\boldsymbol{n}_a$ is the normal vector of section a and the integral path l_a is an arbitrarily chosen loop enclosing the core region of the vortex ring.

Rewriting (3.4) here as

$$\boldsymbol{F}_{\Omega_j} = -\frac{\rho}{2}\frac{\mathrm{d}}{\mathrm{d}t}\oint_{l_j} \boldsymbol{r}\times\left(\iint_a \omega\mathrm{d}A\right)\mathrm{d}\boldsymbol{l}$$

and using (3.5), we obtain

$$\boldsymbol{F}_{\Omega_j} = -\frac{\rho}{2}\frac{\mathrm{d}}{\mathrm{d}t}\left(\Gamma_j\oint_{l_j}\boldsymbol{r}\times\mathrm{d}\boldsymbol{l}\right). \tag{3.6}$$

The projection of $\boldsymbol{F}_{\Omega_j}$ onto the direction $\boldsymbol{n}$ is thus

$$\boldsymbol{F}_{\Omega_j}\cdot\boldsymbol{n} = -\rho\frac{\mathrm{d}}{\mathrm{d}t}(\Gamma_j A_{jn}), \tag{3.7}$$

where $A_{j_n} = \int \mathrm{d}\boldsymbol{A}_j \cdot \boldsymbol{n} = \oint_{l_j} \boldsymbol{r} \times \mathrm{d}\boldsymbol{l} \cdot \boldsymbol{n}$ is the projection of the area enclosed by the vortex ring j along the direction $\boldsymbol{n}$. Here, $\boldsymbol{n}$ can be any direction in which we want to analyse the force component (see figure 5). Since we have assumed a non-decaying circulation, we can rewrite (3.7) as

$$\boldsymbol{F}_{\Omega_j} \cdot \boldsymbol{n} = -\rho \Gamma_j \frac{\mathrm{d}A_{j_n}}{\mathrm{d}t}. \tag{3.8}$$

Hence it is the contraction of the vortex ring in a plane that contributes to the force normal to that plane.

For planar vortex rings as shown in figure 2, area contraction induces a downward force and expansion leads to an upward force (we have adopted the sign convention such that $\Gamma_j < 0$). This important conclusion will be useful for identifying the role of wing plane vortex ring and vortex rings in the wake. For the vortex rings lying in a plane as considered in the present model, if we take $\boldsymbol{n}$ to be the plane normal vector pointing upwards (see figure 2), we have $A_{j_n} = A_j$ where A_j is the area enclosed by the vortex ring, and

$$\boldsymbol{F}_{\Omega_j} \cdot \boldsymbol{n} = -\rho \Gamma_j \frac{\mathrm{d}A_j}{\mathrm{d}t}. \tag{3.9}$$

4. Lift forces due to various vortex rings and time history of the stroke-averaged lift

In this section we will decompose the influence of the vortices on the lift into various sources and study the (stroke-averaged) time evolution of the force starting from the first stroke.

4.1. *Lift forces due to wing-linked vortex ring and wakes*

Using (3.9) for each vortex ring j as displayed in figure 1 and inserting this expression into (3.3), we obtain

$$\boldsymbol{F}_{\Omega} \cdot \boldsymbol{n} = -\rho \sum_j \Gamma_j \frac{\mathrm{d}A_j}{\mathrm{d}t}, \tag{4.1}$$

which, when using $A_j = \pi R_j^2$ for $j \geqslant 1$, can be written as

$$\boldsymbol{F}_{\Omega} \cdot \boldsymbol{n} = -\rho \Gamma_0 \frac{\mathrm{d}A_0}{\mathrm{d}t} - 2\pi\rho \sum_{j \geqslant 1} \Gamma_j R_j u_{Rj}. \tag{4.2}$$

The area variation for the wing-linked vortex ring would be $\mathrm{d}A_0/\mathrm{d}t = 2\pi R_0^2/T$ if it were only due to the sweeping of the wings. However, the vortex rings in the wake also induce an inward velocity for the trailing vortex, which reduces the area at a rate $\pi R_0 u_{R0}$ ($u_{R0} < 0$), where we have assumed a complete circle for the trailing vortex, but with a half circulation or half-time duration, so that

$$\Gamma_0 \frac{\mathrm{d}A_0}{\mathrm{d}t} = \frac{2\pi \Gamma_0 R_0^2}{T} + \pi \Gamma_0 R_0 u_{R0}. \tag{4.3}$$

Inserting the above equation into (4.2) yields

$$\boldsymbol{F}_{\Omega} \cdot \boldsymbol{n} = F_B + F_T + F_W, \tag{4.4}$$

where

$$F_B = -\frac{2\pi\rho \Gamma_0 R_0^2}{T} \tag{4.5}$$

is due to the bound vortex,

$$F_T = -\pi\rho\Gamma_0 R_0 u_{R0}, \tag{4.6}$$

is due to the contraction of the trailing vortex induced by the wake, and

$$F_W = -2\pi\rho \sum_{j\geqslant 1} \Gamma_j R_j u_{Rj} \tag{4.7}$$

is due to the wake vortex ring motion resulting from their mutual induction and the induction of the wing-linked vortex.

With V_m defined by (2.2), we can rewrite (4.5) as

$$\frac{F_B}{R_0} = -2\rho V_m \Gamma_0.$$

Thus we recover the conclusion that 'the bound vortex contributes to lift following the Kutta–Joukowski mechanism'.

Since the inducing effect makes the trailing vortex to contract, from (4.6) we conclude that 'the inducing effect of the wake on the trailing arc reduces the lift', that is $F_T < 0$.

Now consider F_W defined by (4.7). Using (2.8) and (2.10), we obtain

$$\sum_{j\geqslant 1} \Gamma_j R_j u_{Rj} = \sum_{j=1}^{\infty} \Gamma_j R_j u_{0j} + \sum_{j=1}^{\infty} \sum_{k=1,k\neq j}^{\infty} \Gamma_j R_j u_{kj} = \sum_{j=1}^{\infty} \Gamma_j R_j u_{0j},$$

so that the expression (4.7) reduces to

$$F_W = -2\pi\rho \sum_{j=1}^{\infty} \Gamma_j R_j u_{0j}.$$

When further using (2.11), we obtain

$$F_W = \pi\rho\Gamma_0 R_0 u_{R0}. \tag{4.8}$$

Since $u_{R0} < 0$ and $\Gamma_0 < 0$, we conclude that 'the induction on the vortex rings in the wake enhances the lift', that is $F_W > 0$. We must point out that although u_{R0} appears in (4.8), F_W is due to the over all areal variation of the wake vortex rings rather than the trailing arc which has a contracting velocity of u_{R0}. We have known that the contraction of a single vortex ring results in negative lift. The fact that $F_W > 0$ indicates that there must exist a number of vortex rings that expand in the wake.

Actually, in a series of vortex rings, some are contracting while others are expanding. Now we consider the influence of different parts of wake on the lift force when a self-consistent state, for which $\Gamma_j = \Gamma$, is formed in the wake. Firstly, we consider the self-consistent part which is immediately beneath the wing plane. Integrating (3.2) over a half stroke, we obtain the averaged force due to the jth vortex ring

$$\boldsymbol{F}_{w-self_j} = -\frac{2}{T}\int_{t_0}^{t_0+T/2} \rho\Gamma \frac{\mathrm{d}A_j}{\mathrm{d}t}\mathrm{d}t\boldsymbol{n} = -\frac{2\rho\Gamma}{T}(A_j|_{t_0+T/2} - A_j|_{t_0})\boldsymbol{n}.$$

Under the self-consistency assumption, we have $A_j\,|_{t_0+T/2} = A_{j+1}|_{t_0}$, so that the total force due to vortex rings in the self-consistent part of the wake is given by

$$\boldsymbol{F}_{w-self} = -2\rho\Gamma \sum_j \frac{A_j|_{t_0+T/2} - A_j|_{t_0}}{T}\boldsymbol{n} = \frac{2\rho\Gamma}{T}(A_1|_{t_0} - A_\infty|_{t_0+T/2})\boldsymbol{n}. \tag{4.9}$$

Hence, only the areas of the uppermost and the lowermost rings are left in (4.9). In a steady wake, the latter is the area of the ring at the end of the self-consistent part. Denote the area contraction ratio by $\lambda = A_\infty/A_1$, which is normally less than 1, we can rewrite (4.9) as

$$\boldsymbol{F}_{w-self} = \frac{2\rho\Gamma A_1}{T}(1-\lambda)\boldsymbol{n}. \tag{4.10}$$

Hence, $F_{w-self} < 0$ which indicates that the vortex rings close to the wing plane reduce lift.

Although the rings contract immediately after they are shed due to the combined induction of the wing-linked vortex ring and the other vortex rings in the wake, most of them will finally expand after several strokes when they have gone beyond the self-consistent part. It can be observed from figure 4 that the early shed vortex rings below the self-consistent part generally show greater radius than that of the wing-linked ring and rings in the self-consistent part. So the expansion of this part of wake contribute to the lift. Therefore, the overall motion of the wake vortex rings can still lead to lift increasing, that is $F_W > 0$.

Comparing (4.6) with (4.8), we see that 'the force due to the areal contraction of the trailing arc cancels that due to the overall areal expansion of the vortex rings in the wake', so that it holds

$$F_W + F_T = 0. \tag{4.11}$$

4.2. *Time history of the aerodynamic forces*

The aerodynamic force during the initial stage of flapping flight has been studied experimentally by Birch & Dickinson (2001), where it has been shown that lift force experiences a decreasing and increasing process. Here we compute the force for a finite number of vortex rings by

$$\boldsymbol{F}_C(t) = -\rho\sum_{j=0}^{J}\Gamma_j\frac{\mathrm{d}A_j}{\mathrm{d}t}\boldsymbol{n}. \tag{4.12}$$

Similarly as in (4.4), $F_C(t)$ can be decomposed as

$$F_C(t) = F_B(t) + F_T(t) + F_W(t), \tag{4.13}$$

where

$$F_B(t) = -\frac{2\pi\rho\Gamma_0(t)R_0^2}{T} \tag{4.14}$$

is due to the bound vortex,

$$F_T(t) = -\pi\rho\Gamma_0(t)R_0u_{R0}(t) \tag{4.15}$$

is due to the contraction of the trailing vortex induced by the wake, and

$$F_W(t) = -2\pi\rho\sum_{j=1}^{J}\Gamma_jR_ju_{Rj}(t) \tag{4.16}$$

is due to the wake.

When (2.6) along with (2.1*a*) and (2.1*b*) is solved, the new position and radius for each vortex ring are introduced into (4.14), (4.15) and (4.16) to obtain the forces, averaged over each half stroke. The absolute value for each force is not considered

in this paper. Only the relative values defined by

$$\left.\begin{aligned}
\frac{F_B(t)}{F_B(0)} &= \frac{\Gamma_0(t)}{\Gamma_0(0)},\\
\frac{F_W(t)}{F_B(0)} &= \frac{T}{R_0^2}\sum_{j=1}^{J}\frac{\Gamma_j}{\Gamma_0(0)}R_j u_{Rj}(t) = \pi\sum_{j=1}^{J}\frac{\Gamma_j}{\Gamma_0(0)}\bar{R}_j\bar{u}_{Rj}(t),\\
\frac{F_T(t)}{F_B(0)} &= \frac{T}{2R_0^2}\frac{\Gamma_0(t)}{\Gamma_0(0)}R_0 u_{R0}(t) = \frac{\pi}{2}\frac{\Gamma_0(t)}{\Gamma_0(0)}\bar{R}_0\bar{u}_{R0}(t)
\end{aligned}\right\} \tag{4.17}$$

are considered. Here $t=0$ means the first half stroke. For a given f, the computation of the trajectories of the vortex rings gives R_j and u_{Rj} and their normalized values $\bar{R}_j$ and $\bar{u}_{Rj}$.

The variation of $\Gamma_0(t)$, under the present purpose, is due to the downwash velocity induced by the wake. The induced velocity field in the vicinity of the wings has been studied by Sane (2006), who developed a theoretical model to determine the circulation profile along the wing span when the downwash is taken into consideration. The downwash at wing position r in Sane (2006) is induced by the bound vortex located at wing positions other than r. This induced velocity is built ever since the first half stroke, so that it should contribute the same amount in $\Gamma_0(0)$ and $\Gamma_0(t)$. The difference between $\Gamma_0(0)$ and $\Gamma_0(t)$ in the present paper originates from the downwash induced by the previously shed vortex rings in the wake, which has not been mentioned by Sane (2006). The term downwash in the following part, unless otherwise specified, refers to wake-induced downwash velocity.

Now we derive the formula for $\Gamma_0(t)/\Gamma_0(0)$. The circulation on the wing Γ_0 is calculated by $\Gamma_0=\int_0^R\gamma_0(r)\mathrm{d}r$, where γ_0 is the sectional circulation. Using the Prandtl lifting line theory (Prandtl & Tietjens 1957), the sectional circulation at any spanwise position, for an angle of attack α, is related to the sectional lift coefficient $c_l(\alpha)$ by

$$\gamma_0(r)=\frac{1}{2}u(r)c_l(\alpha)c(r), \tag{4.18}$$

where $u(r)=2V_m r/R_0$ is the local free stream velocity and $c(r)$ is the local chord length. In the later calculation, we will take $c(r)=3.2\bar{c}(r/R)^{0.75}(1-r/R)^{0.5}$ (Ellington 1984*a*), which corresponds to the wing tested by Birch & Dickinson (2001), $\bar{c}$ is the mean chord length and R_0 is related to R by $R_0=0.8R$ (Rayner 1979). For the sectional lift coefficient, we use the classical formula $c_l(\alpha)=2\pi\sin(\alpha)$ (Anderson 1991), since we only consider inviscid model in this paper. The effective angle of attack $\alpha=\alpha(r,t)$ is a local one, which is related to the mean effective angle of attack in the first stroke α_0 (geometrical angle of attack subtracted by downwash due to the trailing arc) and wake induced velocity $u_{iw}(r,t)$ by $\alpha(r,t)=\alpha_0-\Delta\alpha_{iw}(r,t)$, where

$$\Delta\alpha_{iw}=\frac{u_{iw}(r,t)}{u(r)}=\frac{\bar{u}_{iw}(r,t)R_0}{2r}$$

is the reduction in angle of attack due to wake and $\bar{u}_{iw}(r,t)=\sum_{j=1}^{J}\bar{u}_{zj}$, with $\bar{u}_{zj}$ given by (2.3*b*), is the induced velocity due to wake. Hence, we have

$$\alpha(r,t)=\alpha_0-\frac{\bar{u}_{iw}(r,t)R_0}{2r}. \tag{4.19}$$

Take sine of (4.19) and use $c_l=2\pi\sin\alpha$, we obtain from (4.18)

$$\gamma_0(r,t)=\frac{2\pi V_m r c(r)}{R_0}\sin(\alpha_0-\Delta\alpha_{iw}). \tag{4.20}$$

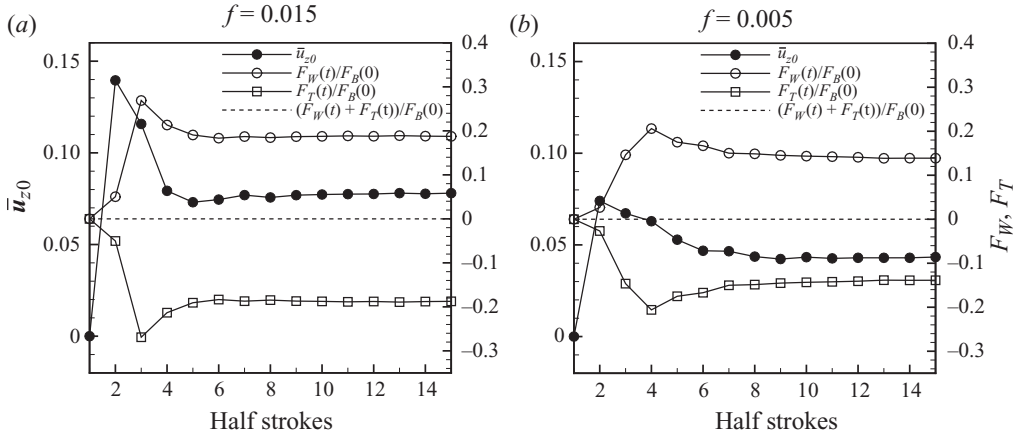

FIGURE 6. Force due to wake and trailing vortex and average induce velocity at wing plane in 15 half strokes with constant circulation for $f = 0.015$ (a) and $f = 0.005$ (b).

In the first half stroke, $u_{iw}(r, 0) = 0$, so

$$\gamma_0(r, 0) = \frac{2\pi V_m r c(r)}{R_0} \sin\alpha_0. \tag{4.21}$$

For the late strokes, since $\Delta\alpha_{iw}$ is small, we have

$$\gamma_0(r, t) = \frac{2\pi V_m r c(r)}{R_0} (\sin\alpha_0 - \cos\alpha_0 \Delta\alpha_{iw}). \tag{4.22}$$

Integrate (4.21) and (4.22) over the span and perform a subtraction, we obtain

$$\frac{\Gamma_0(0) - \Gamma_0(t)}{\Gamma_0(0)} = \cot\alpha_0 \frac{\int_0^R \Delta\alpha_{iw} c(r) r^2 \mathrm{d}r}{\int_0^R c(r) r^2 \mathrm{d}r} = \cot\alpha_0 \frac{R_0}{2} \frac{\int_0^R \bar{u}_{iw}(r, t) c(r) r \mathrm{d}r}{\int_0^R c(r) r^2 \mathrm{d}r}. \tag{4.23}$$

If we define the weighted average downwash velocity at the wing plane $\bar{u}_{z_0}$ as

$$\bar{u}_{z_0}(t) = \frac{R_0}{2} \frac{\int_0^R \bar{u}_{iw}(r, t) c(r) r \mathrm{d}r}{\int_0^R c(r) r^2 \mathrm{d}r}, \tag{4.24}$$

we obtain from (4.23)

$$\frac{\Gamma_0(t)}{\Gamma_0(0)} = 1 - k\bar{u}_{z_0}(t), \tag{4.25}$$

where $k = \cot\alpha_0$. The effective angle of attack in the first stroke is 39° in the experiment of Birch & Dickinson (2001), which corresponds to $k = 1.23$.

Firstly, we assume that all the vortex rings have the same circulation, for which the computed results for the force components $F_W(t)/F_B(0)$ and $F_T(t)/F_B(0)$ and also the average down wash velocity $\bar{u}_{z_0}$ which is related to $F_B(t)/F_B(0)$ through (4.17) and (4.25) in the first 15 half strokes for $f = 0.015$ and 0.005 are shown in figures 6(a) and 6(b), respectively. We observe that these force components vary with time abruptly during the initial stage of flapping, due to strong interactions between the vortex rings.

For $f = 0.015$, the induced velocity $\bar{u}_{z0}$ has a peak value which reduces the wing plane circulation $\Gamma_0(t)/\Gamma_0(0) \sim (1 - k\bar{u}_{z_0})$ to a minimum in the second half stroke. The induced velocity then gradually drops within three half stokes and reach an

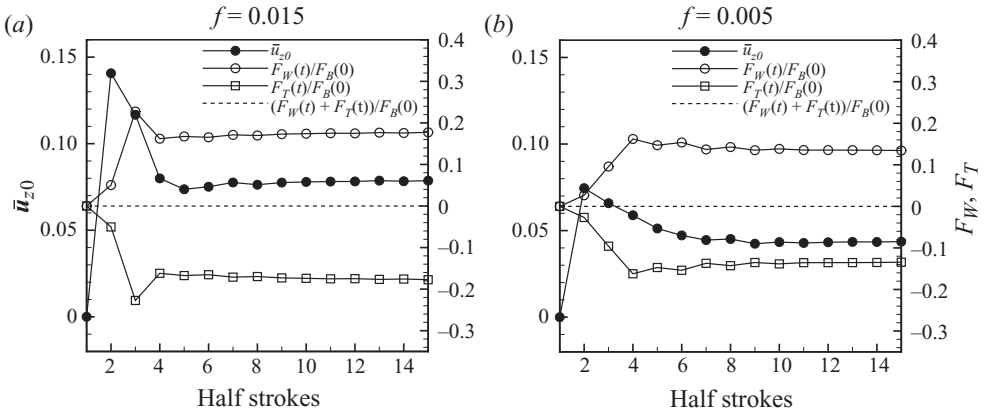

FIGURE 7. Force due to wake and trailing vortex and average induce velocity at wing plane in 15 half strokes with variable circulation when $f = 0.015$ (a) and $f = 0.005$ (b).

asymptotic value of 0.076, which means that the lift force recovers and then almost becomes steady. The steady value of lift force is still less than that of the first half stroke. The lift force due to wake $F_W(t)/F_B(0)$ is always positive and has a peak value of 0.27 at the third half stroke. It then decreases to a value around 0.188 and remains almost constant after the sixth half stroke. The lift of the trailing arc F_T is always negative and displays a trend opposite to F_W. Numerically, we recover $F_W + F_T = 0$ as predicted by the relation (4.11).

The results for $f = 0.005$ are shown in figure 6(b), where the downwash velocity and forces due to trailing arc and the wake are much less than the results for the case of $f = 0.015$. The downwash velocity has a maximum of 0.075 in the second half stroke and then gradually goes down to 0.044 in the following seven to eight half strokes, indicating that more time is required for the wake to become steady for lower f.

In the above we have assumed a circulation Γ_j independent of j. Now we consider the case of variable circulation, due to the induce velocity. At time t_0, we assume that $j-1$ vortex rings have been shed into the wake, so that the circulation of the wing-linked vortex ring $\Gamma_0(t_0)$ is reduced, comparing to $\Gamma_0(0)$, by the induction of the $j-1$ rings in the wake. $\Gamma_0(t_0)$ can be determined using (4.24) and (4.25). After this jth ring is shed into the wake, its circulation remains constant as it moves in the wake. Hence Γ_j constantly equals $\Gamma_0(t_0)$, which is independent of time, but dependent on j. In this way, circulation of each vortex ring Γ_j in the wake is determined in turn before shedding. The results of variable circulation, as displayed in figure 7, are very close to those obtained for constant circulation. The magnitudes of both the peak and steady value of F_W and F_T have slightly decreased, owning to a reduced circulation of the wake vortex rings. For instance, the peak for F_W is 0.227, comparing to 0.27 for constant circulation. The relation (4.11) still holds in the variable circulation case.

Birch & Dickinson (2001) measured the time evolution of the stroke averaged lift force for a dynamically scaled single model wing of a drosophila. The averaged forces are given for each downstroke, that is first, third, fifth and seventh half stroke. Their experimental condition corresponds to $f = 0.0137$ and $k = 1.23$. In figure 8, we display the computed results of $F_B(t)/F_B(0)$ for various f, when $k = 1.23$, including $f = 0.0137$ for drosophila. The normalized value of the experimental result of Birch & Dickinson (2001) is also displayed. We observe that the computed results follow

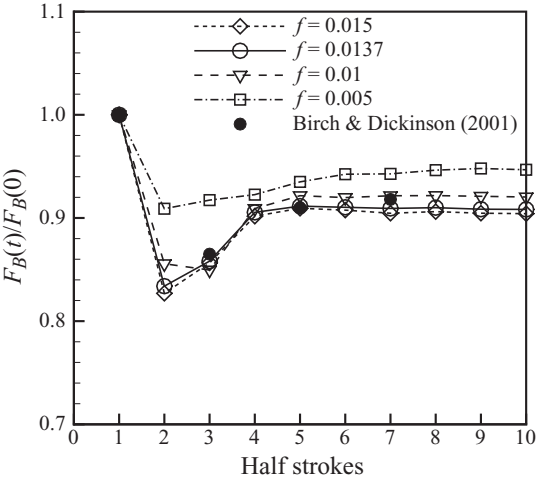

FIGURE 8. Lift force as a function of time for various f when $k = 1.23$. Symbol ● represents the experimental results of Birch & Dickinson (2001).

very well with the experimental observation, though a single wing has been used by Birch & Dickinson (2001). Notably, there is a negative peak at the second (third for the experiment since only the downstroke force is measured) half stroke, and the asymptotic value of $F_B(t)/F_B(0)$ at steady state is 0.91 by computation, comparing to 0.92 measured by Birch & Dickinson (2001).

4.3. *Negative peak of the lift force and their relation to the vortex movement*

Both the experiment of Birch & Dickinson (2001) and our computed results predict a negative peak of lift force at the second half stroke. Now we display the time history of the vortex movement to examine the reason to have such a negative peak. Figure 9(*a–d*) display wake vortex ring trajectories from two to five half strokes in the meridional plane, with the index number indicating j defined in figure 1. The symbols ○ represent vortex ring positions after each stroke. The grey lines are the constant lines for the average downwash velocity at the wing plane induced by a vortex ring of radius r and at a distance z below the wing plane. As a vortex ring travels downwards, its induced velocity at the wing plane drops rapidly.

As is seen in figure 9(*a*), during the second half stroke, the only vortex ring in the wake lies within the close vicinity of the wing plane over the full half stroke and its induced velocity $\bar{u}_{z_0}$ is as large as 0.12 at the end of the second half stroke.

In the third half stroke as displayed in figure 9*b*), two vortex rings coexist in the wake. Due to the downwash flow field already established by the first shed vortex ring and the wing-linked one, both vortex rings move very fast during the early stage of the third stroke. Then, due to their mutual induction, the trajectories of these two vortex rings round one about the other, reaching a position near $z \sim 0.4R_0$ at the end of this half stroke. The two vortex rings induce a downwash velocity around $0.06 + 0.045 = 0.105$, a value slightly smaller than at the second half stroke, meaning that the lift starts to recover.

In the fourth half stroke (figure 9*c*), the previously shed vortex rings (vortex ring 2 and 3) still lie outside the tube defined by $r \leqslant R_0$, so that the newly shed vortex $j = 1$ undergoes a very large downwards velocity. At the end of the fourth half stroke, the vortex ring 1 is at the position around $0.8R_0$, with an induced velocity at the

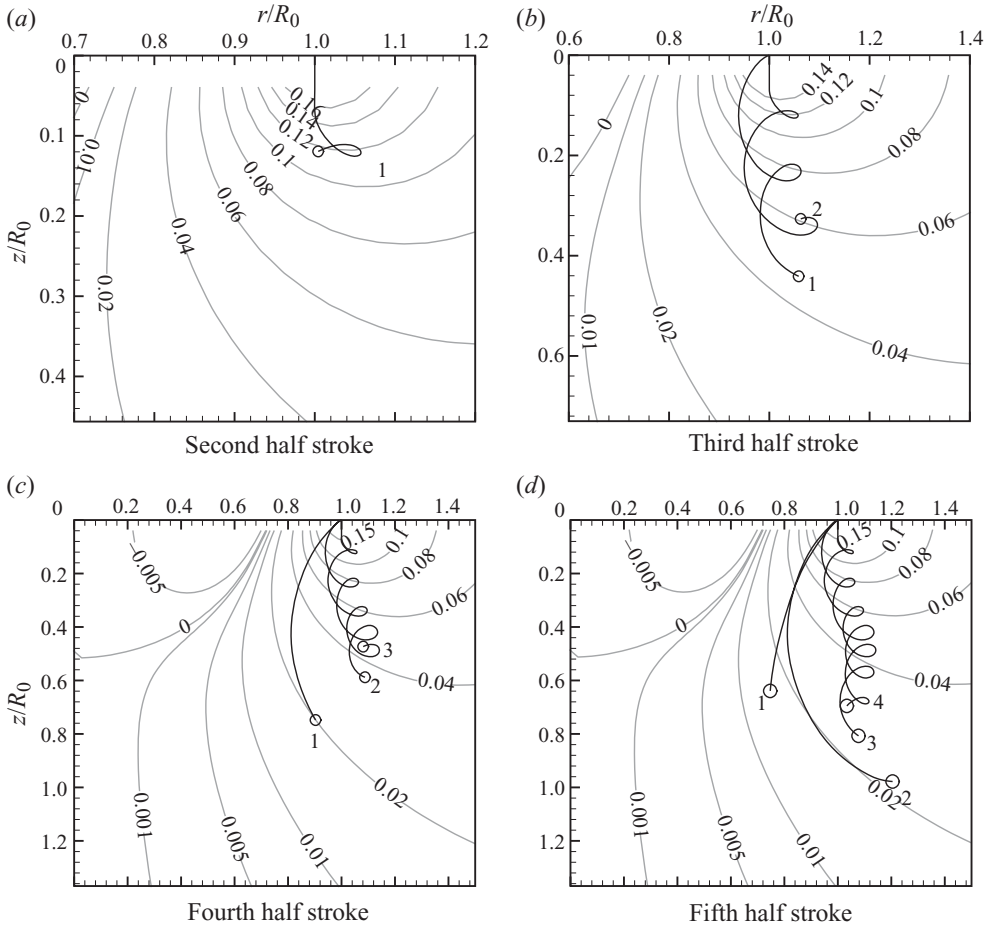

FIGURE 9. Vortex ring trajectories superimposed on the constant lines of downwash velocity $\bar{u}_{z0}$ at the wing plane for $f = 0.0137$. Symbols ○ represent wake vortex ring positions at the end of a half stroke and the numbers indicate ring indices j.

plane close to 0.02. The early two vortex rings lie at positions with a total inducing velocity (at wing plane) about $0.04+0.035 = 0.075$. Hence, the total downwash velocity induced by the three vortex rings decreases to 0.095.

Figure 9(*d*) displays the trajectories for the fifth half stroke where we have four shed vortex rings. Due to the mutual inducing effect, the newly shed vortex rings move downward very fast, so that their effective induction on the wing plane is very weak. Since the early shed vortex rings are far below the wing plane and the newly shed vortex rings move along an orderly path after the wake has become steady, the induced velocity gradually recovers to an asymptotic value.

In summary, the negative peak for the lift at the second half stroke is attributed to the earliest shed vortex ring which lies in the very close vicinity of the wing plane thus inducing a very large downwash velocity. After the second half stroke, this earliest and newly shed vortex rings move fast to a position far below the wing plane so that the downwash velocity on the wing plane by all the vortex rings in the wake is smaller than that by the single vortex ring at the second stroke.

5. Concluding remarks and perspectives

Through applying the vorticity moment theory to the flapping flight vortex model of Rayner (1979) and Ellington (1984*b*), we have identified the roles of the various vortex sources on the stroke-averaged lift forces. The specific conclusions are summarized below:

(*a*) In general, the areal contraction or expansion of a vortex ring in the fluid reduces or enhances the lift. The downwash or upwash velocity induced by a vortex ring on the wing plane reduces or enhances the lift.

(*b*) The bound vortex of each wing contributes to the conventional lift following the Kutta–Joukowski mechanism.

(*c*) The contraction of the trailing arc, induced by the wake, reduces the lift by an amount of the order of 20 % of the conventional lift, and the induction on the wake increases the lift by the same amount, so that the areal contraction or expansion of vortex rings on the wing plane and in the wake does not have a direct effect on the lift (though indirectly through changing the amount of downwash velocity).

(*d*) Most importantly, the wake reduces the lift, by an amount close to 10 % for a feathering parameter $f = 0.0137$, through inducing a downwash velocity on the wing plane. The lift force drops to a minimum at the second half stroke, and then increases to an asymptotic value about 10 % below the lift at the first half stroke. This trend follows very well with the experimental observation of Birch & Dickinson (2001). Decreasing f reduces the value peak (i.e. elevate the negative peak value) and increases the steady lift.

(*e*) The existence of the negative peak of lift at the second half stroke is due to the first shed vortex ring which, just at the second half stroke, lies in the close vicinity to the wing plane, leading to a peak of the wing plane downwash velocity. After the second half stroke, this first and newly shed vortex rings move fast to a position far below the wing plane so that the downwash velocity on the wing plane by all the vortex rings in the wake is smaller than that by the single vortex ring at the second stroke.

These conclusions have been drawn based on the ideal vortex model of Rayner (1979) and Ellington (1984*b*), dropping out the possible coupling with other effects such as wing rotation, acceleration, etc. The conclusions seem to be useful for identifying the relative importance of vortex patterns. Below are topics that deserve further study.

Shape and configuration of the vortex rings. We have assumed that a single ring is shed per stroke and that all the vortex rings are circular and lie in a horizontal plane. According to experimental results, the vortex rings would be non-planar and non-circular with a more complicated structure. For some species, like bats and hummingbirds, a double vortex loops model may have to be used.

Unsteady lift force. The unsteadiness of the aerodynamic forces in each stroke is due to the acceleration, wing rotation, etc. (Sane 2003), the mutual interaction between the vortex rings and the other unsteady processes would induce further unsteadiness. As we have noted in § 2.3, the bounding vortex segments will pass any point of the wing plane at two instants of equal duration but with opposite signs, its inducing effect on the wake, though negligible when stroke-averaged, may induce unsteadiness inside each stroke.

Image effects of the wake. The images of the vortex rings in the insect body and with respect to the wing would change the lift through inducing further downwash velocity and areal contraction of the real vortex rings. This will be considered in a forthcoming paper.

Forward flight and other similar problems. During the forward flight of hawkmoth, the near-field vortex wake appears to resemble elliptical vortex rings according to the digital particle image velocimetry (DPIV) experiments (Bomphrey *et al.* 2006). This could be studied by using elliptical vortex rings in an incoming flow field. Wing rotation problems and falling of cards in tumbling motion also involve shedding of vortex rings (Willmarth, Hawk & Harvey 1964; Hans 1983; Andersen, Pesavento & Wang 2005) and the roles of these vortex rings can be similarly analysed.

Decay of circulation. Viscous diffusion of the vortex core of each vortex ring may result in circulation decay due to the vorticity cancellation in the ring centreline. For a single and free vortex ring the circulation decays as (Fukumoto & Kaplanski 2008) $\Gamma = \Gamma_0(1 - \exp(-R_0{}^2/4\nu t))$, where R_0 is the radius of the ring, Γ_0 is the initial circulation and ν is the kinematic viscosity of the fluid. For a period $T = 0.02$ s and stroke plane radius 10^{-2} m, typical to insect flight, the above formula shows a decay of 1 % after 10 half stokes. For a system of vortex rings no study is found for the decay of circulation. Further study on decaying vortex rings should be considered.

The authors are grateful to the referees for many valuable suggestions. Notably, their comments lead to a better derivation of (4.25). This work has been supported by the 211 and the 985 Program of Tsinghua University, and partially supported by the Chinese NSF Contract No. 10972116.

REFERENCES

Altshuler, D. L., Princevac, M., Pan, H. & Lozano, J. 2009 Wake patterns of the wings and tail of hovering hummingbirds. *Exp. Fluids* **46**, 835–846.

Anderson, J. D. 1991 *Fundamentals of Aerodynamics*. McGraw-Hill.

Andersen, A., Pesavento, U. & Wang, Z. J. 2005 Unsteady aerodynamic of fluttering and tumbling plates. *J. Fluid Mech.* **541**, 65–90.

Ansari, S. A., Zbikowski, R. & Knowles 2006 Aerodynamic modelling of insect-like flapping flight for micro air vehicles. *Prog. Aerosp. Sci.* **42**, 129–172.

Aono, H., Liang, F. & Liu, H. 2008 Near- and far-field aerodynamics in insect hovering flight: an integrated computational study. *J. Exp. Biol.* **211**, 239–257.

Batchelor, G. K. 1967 *An Introduction to Fluid Dynamics*. Cambridge University Press.

Bergou, A. J., Xu, S. & Wang, Z. J. 2007 Passive wing pitch reversal in insect flight. *J. Fluid Mech.* **591**, 321–337.

Birch, J. M. & Dickinson, M. H. 2001 Spanwise flow and the attachment of the leading-edge vortex on insect wings. *Nature* **412**, 729–733.

Birch, J. M., Dickson, W. B. & Dickinson, M. H. 2004 Force production and flow structure of the leading edge vortex on flapping wings at high and low Reynolds numbers. *J. Exp. Biol.* **207**, 1063–1072.

Bomphrey, R. J., Lawson, N. J., Taylor, G. K. & Thomas, A. L. R. 2006 Application of digital particle image velocimetry to insect aerodynamics: measurement of the leading-edge vortex and near wake of a hawkmoth. *Exp. Fluids* **40**, 546–554.

Dickinson, M. H., Lehmann, F.-O. & Sane, S. P. 1999 Wing rotaition and the aerodynamic basis of insect flight. *Science* **284**, 1954–1960.

Ellington, C. P. 1984*a* The aerodynamics of hovering insect flight. Part II. Morphological parameters. *Phil. Trans. R. Soc. Lond.* B **305**, 17–40.

Ellington, C. P. 1984*b* The aerodynamics of hovering insect flight. Part V. A vortex theory. *Phil. Trans. R. Soc. Lond.* B **305**, 115–144.

Ellington, C. P., van den Berg, C., Willmott, A. P. & Thomas, A. L. R. 1996 Leading-edge vortices in insect flight. *Nature* **384**, 626–630.

Fukumoto, Y. & Kaplanski, F. 2008 Global time evolution of an axisymmetric vortex ring at low Reynolds numbers. *Phys. Fluids* **20**, 053103.

Gerz, T., Holzäpfel, F. & Darracq, D. 2002 Commercial aircraft wake vortices. *Prog. Aerosp. Sci.* **38**, 181–208.

Hans, J. L. 1983 Autorotation. *Annu. Rev. Fluid Mech.* **15**, 123–147.

Kokshaysky, N. V. 1979 Tracing the wake of a flying bird. *Nature* **279**, 146–148.

Lauder, G. V. 2001 Flight of the robofly. *Nature* **412**, 688–689.

Lehmann, F.-O. 2004 The maechanisms of lift enhancement in insect flight. *Naturwissenschaften* **91**, 101–122.

Lehmann, F.-O. 2008 When wings touch wakes: understanding locomotor force control by wake-wing interference in insect wings. *J. Exp. Biol.* **211**, 224–233.

Maxworthy, T. 1972 The structure and stability of vortex rings. *J. Fluid Mech.* **51**, 15–32.

Maxworthy, T. 1981 The fluid dynamics of insect flight. *Annu. Rev. Fluid Mech.* **13**, 329–350.

Miller, L. A. & Peskin, C.S. 2005 A computational fluid dynamics of 'clap and fling' in the smallest insects. *J. Exp. Biol.* **208**, 195–212.

Prandtl, L. & Tietjens, O. K. G. 1957 *Applied Hydro- and Aeromechanics: Based on Lectures of L. Prandtl*. Dover.

Ramamurti, R. & Sandberg, W. C. 2007 A computational investigation of the three-dimensional unsteady aerodynamics of drosophila hovering and maneuvering. *J. Exp. Biol.* **210**, 881–896.

Rayner, J. M. V. 1979 A vortex theory of animal flight. Part 1. The vortex wake of a hovering animal. *J. Fluid Mech.* **91**, 697–730.

Sane, S. P. 2003 The aerodynamics of insect flight. *J. Exp. Biol.* **206**, 4191–4208.

Sane, S. P. 2006 Induced airflow in flying insects. Part I. A theoretical model of the induced flow. *J. Exp. Biol.* **209**, 32–42.

Sane, S. P. & Dickinson, M. H. 2001 The control of flight force by a flapping wing: lift and drag production. *J. Exp. Biol.* **204**, 2607–2626.

Sane, S. P. & Dickinson, M. H. 2002 The aerodynamic effects of wing rotation and a revised quasi-steady model of flapping flight. *J. Exp. Biol.* **205**, 1087–1096.

Spedding, G. R. 1986 The wake of a jackdaw (corvus monedula) in slow flight. *J. Exp. Biol.* **125**, 287–307.

Sun, M. & Tang, J. 2002 Unsteady aerodynamics force generation by a model fruit-fly wing. *J. Exp. Biol.* **205**, 55–70.

Traub, L. W. 2004 Analysis and estimation of the lift components of hovering insects. *J. Aircr.* **41**, 284–289.

Wang, Z. J. 2005 Dissecting insect flight. *Annu. Rev. Fluid Mech.* **37**, 183–210.

Weis-Fogh, T. 1973 Quick estimates of flight fitness in hovering animals, including novel mechanisms for lift production. *J. Exp. Biol.* **59**, 169–230.

Willmarth, W. W., Hawk, N. E. & Harvey, R. L. 1964 Steady and unsteady motions and wakes of freely falling disks. *Phys. Fluids* **7**, 197–208.

Wu, J. C. 1981 Theory for aerodynamic force and moment in viscous flows. *AIAA J.* **19**, 432–441.